ELSEVIER

Journal of Alloys and Compounds 452 (2008) 343–347

Journal of ALLOYS AND COMPOUNDS

www.elsevier.com/locate/jallcom

Quasicrystalline phase in melt-spun Al–Mn–Be ribbons

Franc Zupanič [a,*], Tonica Bončina [a], Alojz Križman [a], Werner Grogger [b], Christian Gspan [b], Boštjan Markoli [c], Savo Spaić [c]

[a] *University of Maribor, Faculty of Mechanical Engineering, Smetanova 17, SI-2000 Maribor, Slovenia*
[b] *Research Institute for Electron Microscopy, Graz University of Technology, Steyrergasse 17, A-8010 Graz, Austria*
[c] *University of Ljubljana, Faculty of Natural Sciences and Engineering, Aškerčeva 12, SI-1000 Ljubljana, Slovenia*

Received 6 October 2006; received in revised form 9 November 2006; accepted 10 November 2006
Available online 19 December 2006

Abstract

The quasicrystalline phase in melt-spun Al–Mn–Be alloys was investigated. In ribbons 40–60 μm thick the phase was present in the form of small particles rather uniformly dispersed in an aluminium solid solution matrix. The quasicrystalline phase had a primitive icosahedral structure. It was confirmed that it contained a substantial amount of Be. Nonetheless, it seemed that the electron-to-atom ratio remained close to that of binary $Al_{80}Mn_{20}$ quasicrystal.

Keywords: Quasicrystals; Rapid solidification; Microstructure; Metallography; Electron emission spectroscopies

1. Introduction

Quasicrystals are solids with a highly ordered but non-periodic arrangement of atoms [1]. Since their discovery [2] they have been studied very intensively. Today, many interesting properties of quasicrystalline materials are known, and attention has shifted from fundamental research to application of quasicrystals in engineering [3–6].

Quasicrystals can be used in the form of strengthening particles in aluminium-based alloys. Up until now several aluminium alloys were developed enabling such strengthening [7,8].

Until recently not much attention was given to the Al–Mn–Be alloy system. However, it was discovered that beryllium strongly increased the quasicrystalline forming ability in well-known Al–Mn quasicrystalline alloys [9–11]. The metastable quasicrystalline phase was present in the microstructure even when conventional casting methods were used; with relatively slow cooling rates in the range of 100 K/s. The main argument for explaining this behaviour was the assumption that beryllium replaces aluminium in the quasicrystalline phase. However, no clear evidence was given for this assumption, except that investigated Be containing alloys were mainly composed of a ternary quasicrystalline phase. Based on this, the focus of our research was directed to the quasicrystalline phase in melt-spun Al–Mn–Be alloys, with the main aim of determining the beryllium content in quasicrystals.

2. Experimental

Two Al–Mn–Be alloys were prepared using Al 99.99 and Al–Mn and Al–Be master alloys containing 30 mass% Mn and 5.5 mass% Be, respectively. The nominal composition of the first alloy was 5 at.% Be, 3 at.% Mn, 92 at.% Al (M5), and of the second alloy 5 at.% Be, 6 at.% Mn and 89 at.% Al (M10). Note the same content of Be in both alloys. Two times higher content of Mn in M10 compared to M5 was chosen in order to obtain higher fraction of quasicrystalline particles in melt spun ribbons. The alloys were vacuum induction melted and cast into rods with 50 mm diameter. The rods were cut to appropriate lengths and melt spun in Melt spinner 30 M, Marko Inc. Typical melt-spun conditions were: BN-protected graphite crucible with 1 mm orifice, wheel speed 25 m min^{-1}, casting temperature 900–950 °C. For this investigation only ribbons with thicknesses from 40 to 60 μm were selected. The chemical compositions of the melt spun ribbons were determined using ICP-AES (inductively coupled plasma-atomic emission spectroscopy) and are given in Table 1. It is evident that they slightly deviate from the nominal compositions.

For the characterisation of the investigated alloys several microstructural characterisation techniques were used. Light microscopy (LM) was made on a Nikon Epiphot 300, and scanning electron microscopy (SEM) on a SEM JEOL JSM 840 A and FEI SIRION 400 NC. The specimens for LM and SEM were mounted in Struers Resin 3, mechanically grinded and polished. Etching for LM was performed using a solution of 2 g NaOH and 4 g Na_2CO_3 in 94 ml H_2O, and deep etching for SEM with a mixture of 5 ml HNO_3, 2.5 ml HCl and 1 drop

* Corresponding author. Tel.: +386 2 220 7863; fax: +386 2 220 7990.
E-mail address: franc.zupanic@uni-mb.si (F. Zupanič).

0925-8388/$ – see front matter © 2006 Elsevier B.V. All rights reserved.
doi:10.1016/j.jallcom.2006.11.041

of HF. Transmission electron microscopy (TEM) was carried out on a Philips CM20 and a JEOL 2000 FX. The TEM specimens for the Philips CM20 were cut out at specific sites using the focussed ion beam (FIB) in an FEI Nova 200 Nanolab, and for the JEOL 2000 FX specimens were prepared using the ion beam etching and polishing system GATAN PIPS 691 (3 keV, angle ±2–5°). Energy dispersive spectroscopy (EDS) was carried out both in SEM and TEM. Electron energy loss spectroscopy (EELS), energy-filtering TEM (EFTEM) and high-resolution transmission electron microscopy (HRTEM) was done on an FEI Technai F20. X-ray diffraction (XRD) was carried out on a Siemens D-5000, using Cu Kα1-radiation, with a scan rate of 0.025°/s in the range of 20°–80°. Auger electron spectroscopy (AES) was carried out in a Microlab 310-F. The energy of the primary electrons was 10 keV, electron current 10 nA and electron beam diameter 10 nm. Specimens were etched with argon ions for approximately 1.5 h to remove a surface oxide layer, prior to analysis.

3. Results and discussion

Fig. 1 shows the microstructure of a melt-spun ribbon which is typical of both alloys with thicknesses between 40 and 60 μm. Two regions (A and B) can clearly be observed. The region A is the wheel-side, and region B the air-side of the ribbon. Using LM, region A appeared almost featureless, but a relatively uniform distribution of quasicrystalline particles was observed in region B. SEM-images of region A revealed a very uniform distribution of nanoscale-sized quasicrystalline particles. On the other hand the quasicrystalline particles in region B were much larger, up to 500 nm; the particles with diameters up to 200 nm were apparently spherical, but the larger particles showed preferential growth in some directions and they appeared dendritic. The difference in microstructure can be attributed to different cooling rates since EDS of both regions did not revealed any variation in chemical composition from the wheel-side toward the air-side of the ribbons. The microstructure of the ribbons indicated that quasicrystalline particles formed directly from the melt. Subsequently, Al-solid solution phase nucleated on the wheel, propagated with the planar interface morphology up to the air-side of the ribbon and engulfing the quasicrystalline particles. It is very probable that the region A solidified before and the region B after the occurrence of the recalescence. As a result, the quasicrystalline particles in the region B were much larger because they were subjected to coarsening during recalescence.

Fig. 2 shows an individual quasicrystalline particle in region B with corresponding diffraction patterns with two-fold, three-fold and five-fold symmetry axes. The position of the most important diffraction spot (2 1 1 1 1 1) in the Elser's indexing scheme [12] indicated that the quasicrystalline phase possessed primitive icosahedral structure; which was also found by Kim et al. [11].

Fig. 3 shows the HRTEM image of a quasicrystalline particle taken in a five-fold symmetry axis. We can clearly see spots of different brightness forming five sets of virtual parallel lines with a mutual orientation of 72°. By drawing an appropriately

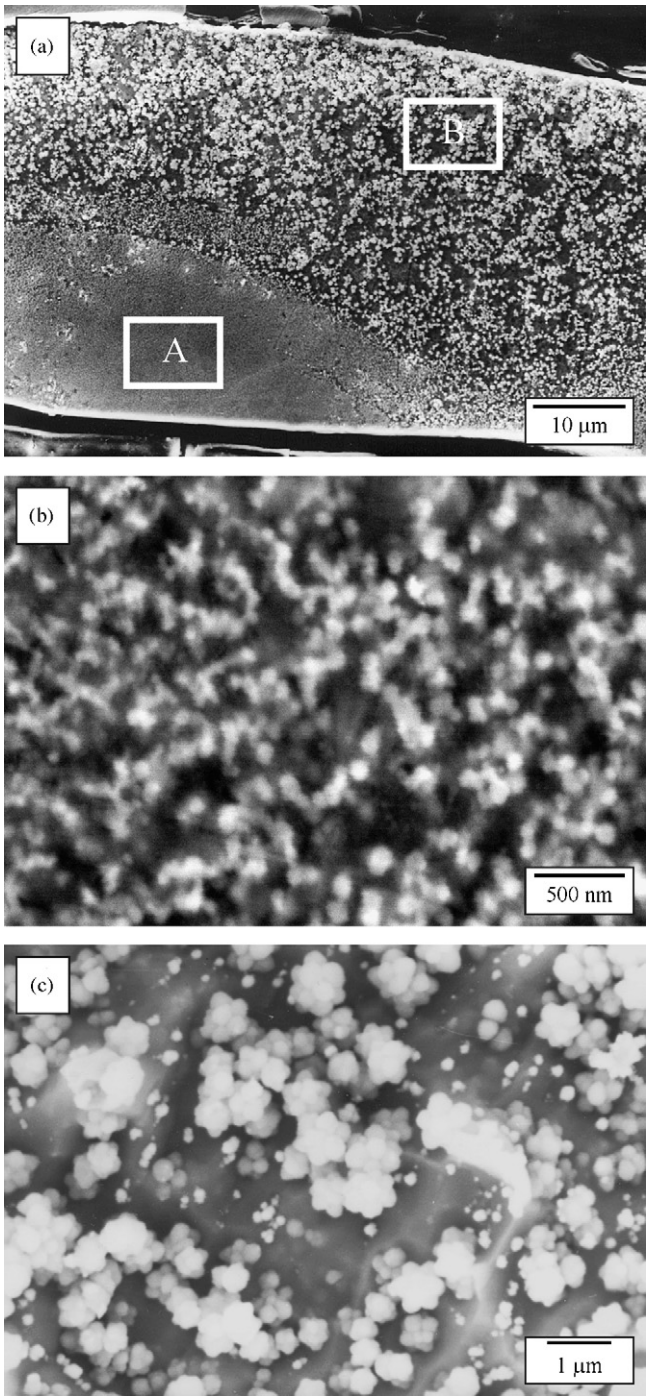

Fig. 1. (a) Typical microstructure of melt-spun ribbons (alloy M10). (b) High-resolution SEM image of region A in (a), and (c) high resolution SEM image of region B in (a).

Table 1
Chemical composition of the Al–Mn–Be melt spun ribbons (ICP-AES)

Alloy	Al (mass%)	Al (at.%)	Mn (mass%)	Mn (at.%)	Be (mass%)	Be (at.%)
M5	92.5	92.5	6.0	3.0	1.5	4.5
M10	86.9	88.6	11.1	5.6	1.9	5.8

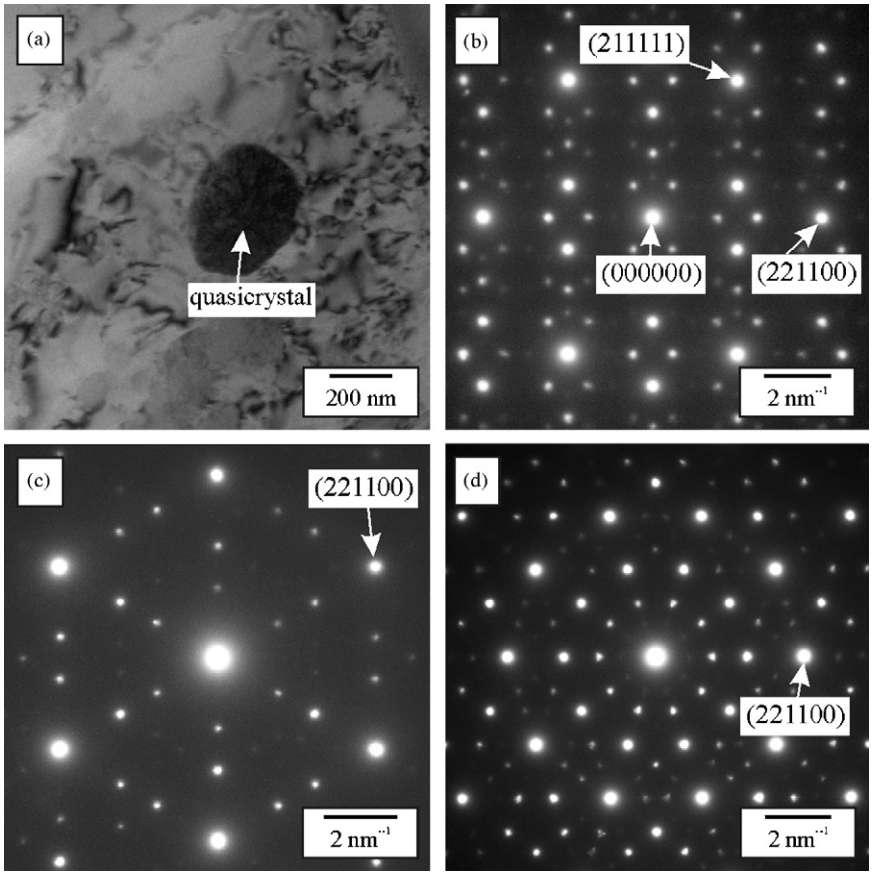

Fig. 2. (a) TEM micrograph of an individual quasicrystalline particle in Al-rich matrix in alloy M5. SAED-patterns taken along (b) two-, (c) three- and (d) five-fold axis of the quasicrystalline particle.

oriented pentagon all virtual lines appeared parallel to the sides of pentagon. This is completely consistent with the icosahedral five-fold symmetry and the FFT (fast Fourier transform). In Fig. 3 a set of parallel line segments is shown. The ratio L to S equals τ (golden mean = 1.618...), which is also typical for quasicrystals. However, the quantitative interpretation of HRTEM images of quasicrystals depends strongly on specimen thickness [13] therefore it is not possible to obtain the atomic positions from the HRTEM-image without modelling. Namely, dynamical diffraction effects can generate extra spots, leading to new diffraction patterns of reduced scale but similar symmetry therefore not automatically distinguishable from the kinematical ones.

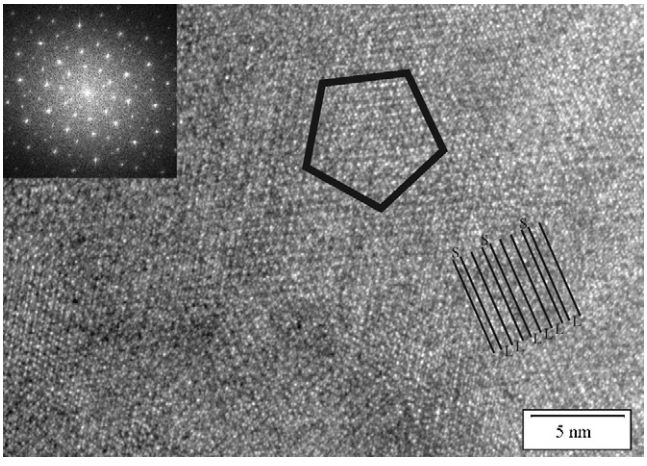

Fig. 3. HRTEM of a quasicrystalline particle in a five-fold orientation with corresponding FFT insert (fast Fourier transform). Alloy M5.

For the determination of the chemical composition of the matrix and particles of the quasicrystalline phase, as well as for distribution of elements EDS (both in SEM and TEM), EFTEM, and AES were used. The results of EDS and EFTEM showed that manganese is concentrated in the quasicrystalline phase (Fig. 4), whereas both methods failed to detect beryllium. EDS in TEM revealed a weight ratio Mn/Al around 0.4 in the particles and 0.02 in the matrix. In AES derivative spectra of the matrix no Be peak could be observed indicating that its content should be below the detection limit. Typically, it is few tenths of the atomic percent [14], and in this range is also Be equilibrium maximum solubility (0.3 at.% or 0.1 mass%, [15]). Therefore we can conclude that no substantial supersaturation of Be in Al-rich solid solution was obtained by melt-spinning. On the other hand AES showed that Mn content in Al-rich solid solution was approximately 6 at.% (3 mass%). The results of EDS in TEM and AES indicate that in the melt-spun ribbons the Al-rich solid solution was supersaturated with Mn since its equilibrium maximum solubility is 1.25 mass% (0.62 at.%) [16].

With AES we analysed many particles with the sizes around 500 nm in diameter in both alloys. Fig. 5 shows two typical

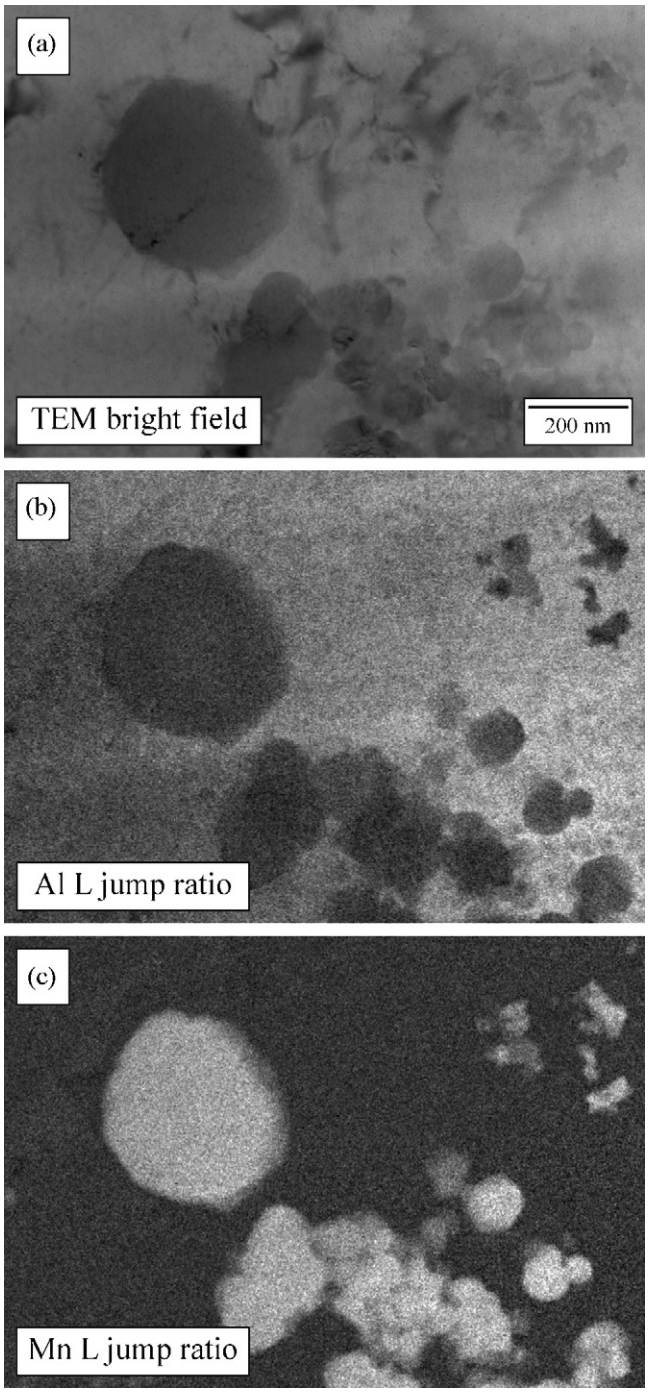

Fig. 4. Distribution of elements using EFTEM in alloy M5. (a) TEM bright-field image, zero-loss filtered, (b) elemental distribution of Al and (c) elemental distribution of Mn (jump ratio images).

AES derivative spectra of quasicrystalline particles in alloys M5 and M10. Peaks of all alloying elements (Be, Al and Mn) can be clearly seen. The Be-peak appeared at 101 eV and was very pronounced. The method of quantitative analysis was peak-to-peak height measurements from derivative spectra and the sensitivity factors characteristic for the employed instrument were used. Since we did not have available standards with concentrations close to those of the actual specimens we estimate that the accuracy of measurements for all elements was ±20%

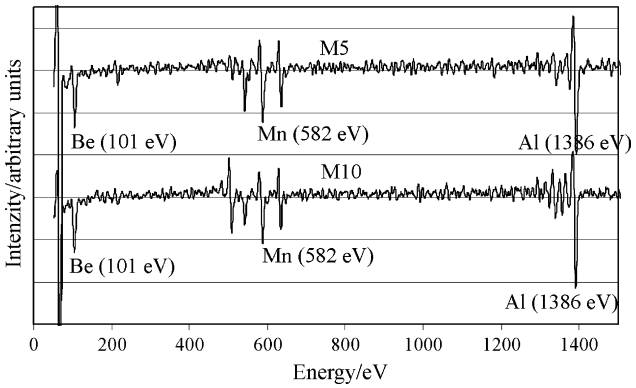

Fig. 5. Auger electron derivative spectra of quasicrystalline particles in melt-spun ribbons of alloys M5 and M10 (M5: 40.58 at.% Be, 14.24 at.% Mn, 45.18 at.% Al; *e/a* = 1.65, M10: 38.33 at.% Be, 13.53 at.% Mn, 47.65 at.% Al; *e/a* = 1.70).

[14]. The content of Mn was between 14 and 16 at.% Mn, the Be-content was in the range between 30 and 40 at.% Be and the remaining part was aluminium. The compositions of the analysed quasicrystalline particles were almost the same in both alloys; despite that alloy M10 contained much more Mn and consequently also a higher fraction of the quasicrystalline phase. The average composition was 35 at.% Be, 15 at.% Mn and 50 at.% Al. The electron-to-atom ratio *e/a* for this composition was 1.65 (valences of Be, Al and Mn were taken +2, +3 and −3.66, respectively [17]). By taking into account the accuracy of measurements (±20%) electron-to-atom ratio lied in the range between 1.40 and 1.90. This is typical for spd quasicrystals (Mackay type, the most frequent values of *e/a* are between 1.7 and 1.9 [15]), to which binary Al–Mn quasicrystals belong. That means that Be can substitutionally replace Al in the quasicrystalline phase to a great extend. Namely, it has a smaller atomic radius *R* than aluminium, but the same electronegativity χ (R_{Be} = 111.3 pm, R_{Al} = 143.2 pm, R_{Mn} = 136.7 pm, χ_{Be} = 1.5, χ_{Al} = 1.5, χ_{Mn} = 1.6). In the melt spun ribbons only quasicrystalline phase was observed in the Al-rich solid solution matrix. However, Raynor et al. [18] discovered ternary $Al_{15}Mn_3Be_2$ phase, which is believed to be one of the equilibrium phases in the Al–Mn–Be system [19]. The electron-to-atom ratio for this alloy is 1.9, which is in the range of spd quasicrystals. We may speculate that by melt spinning of the melt with composition of the $Al_{15}Mn_3Be_2$ phase a quasicrystalline phase would form.

It is known that the electron-to-atom ratio *e/a* plays an important role in the stabilization of quasicrystalline phases [15]. In the Al–Mn system the amount of Mn in quasicrystals ranges from 10 to 20 wt.%. The large amount of Be in the alloy strongly enhances the formation of quasicrystals, shifting the formation-region to very small amounts of Mn. Kim et al. [11] argued that the electron-to-atom ratio *e/a* for $Al_{79.9}Mn_{13.5}Be_{6.6}$ quasicrystal lied around 2.03. They suggested the existence of a new type of quasicrystal having *e/a* between 2.0 and 2.2, which is close to Frank-Kasper type quasicrystals [17]. However, our investigation did not confirm their findings. The electron-to-atom ratios for quasicrystals in both M5 and M10 were almost the same as in pure Al–Mn. However, it seems that with the incorporation of Be into the quasicrystalline phase

the composition of the phase changes, especially the fraction of Al, so that the *e*/*a* ratio remains almost unchanged. Yet our results do not exclude the possibility that in Al–Mn–Be alloys two different quasicrystalline phases may form, which depends on the alloy composition, cooling rate and perhaps also on the relative fraction between the Al-rich solid solution and the quasicrystalline phase.

4. Conclusions

The results of this work lead us to the following conclusions.

Melt-spun ribbons with thicknesses between 40 and 60 μm consisted of quasicrystalline particles rather evenly distributed in an Al-rich solid solution matrix.

The structure of the quasicrystalline phase in melt-spun Al–Mn–Be alloys was primitive icosahedral.

Both beryllium and manganese were enriched in the quasicrystalline particles. However, the quasicrystalline particles contained a substantial amount of Be (∼35 at.%), but it seemed that the electron-to-atom ratio remained close to that of binary $Al_{80}Mn_{20}$ quasicrystal.

Therefore, it was confirmed that the increased quasicrystal forming ability of Al–Mn alloys containing beryllium could be attributed to its presence in the quasicrystalline phase.

Acknowledgement

This work was partly financed by the research programme: Technologies of Metastable Metallic Materials at Slovenian Ministry of Higher Education and Science.

References

[1] S.V. Divinski, Scr. Mater. 34 (1996) 1351–1355.
[2] D. Shechtman, I. Blech, D. Gratias, J.W. Cahn, Phys. Rev. Lett. 53 (1984) 1951–1953.
[3] J.-M. Dubois, Mater. Sci. Eng. A 294–296 (2000) 4–9.
[4] A. Singh, M. Nakamura, M. Watanabe, A. Kato, A.P. Tsai, Scr. Mater. 49 (2003) 417–422.
[5] S. Yi, K.B. Kim, W.T. Kim, D.H. Kim, Scr. Mater. 44 (2001) 1757–1760.
[6] A. Inoue, T. Zhang, S. Ishihara, J. Saida, M. Matsushita, Scr. Mater. 44 (2001) 1615–1619.
[7] A. Inoue, H. Kimura, J. Light Metals 1 (2001) 31–41.
[8] F. Schurack, J. Eckert, L. Schultz, Acta Mater. 49 (2001) 1351–1361.
[9] G.S. Song, E. Fleury, S.H. Kim, W.T. Kim, D.H. Kim, J. Alloys Compd. 342 (2002) 251–255.
[10] G.S. Song, E. Fleury, S.H. Kim, W.T. Kim, D.H. Kim, J. Mater. Res. 17 (2002) 1671–1677.
[11] S.H. Kim, G.S. Song, E. Fleury, K. Chattopadhyay, W.T. Kim, D.H. Kim, Philos. Mag. A 82 (2002) 1495–1508.
[12] V. Elser, Phys. Rev. B 32 (1985) 4892–4898.
[13] A. Howie, in: P. Buseck, J. Cowley, L. Eyring (Eds.), High-resolution Transmission Electron Microscopy and Associated Techniques, Oxford University Press, New York, 1992, pp. 607–632.
[14] B. Doyle, F.D. McDaniel, in: E.N. Kaufmann (Ed.), Characterisation of Materials, vol. 2, John Wiley & Sons, Inc., Hoboken, pp. 1157–1174.
[15] J.L. Murray, D.J. Kahan, in: T.B. Massalski (Ed.), Binary Alloy Phase Diagrams, 2nd Ed., ASM International, 1990, pp. 125–128.
[16] A.J. McAlister, J.L. Murray, in: T.B. Massalski (Ed.), Binary Alloy Phase Diagrams, 2nd Ed., ASM International, 1990, pp. 171–174.
[17] G. Trambly de Laissardiere, D. Nguyen-Manh, D. Mayou, Prog. Mater. Sci. 50 (2005) 679–788.
[18] G.V.S. Raynor, C.R. Faulkner, J.D. Noden, A.R. Harding, Acta Metall. 1 (1953) 629–648.
[19] L.F. Mondolfo, Aluminium Alloys: Structure and Properties, Butterworths, 1976, pp. 447–448.